Compact Air-Core Inductors for Variable Frequency Soft-Switching in 3 Phase Inverters

Youssef A Fahmy
Dept. of Electrical Engineering
Columbia University
New York, USA
y.fahmy@columbia.edu

Matthias Preindl
Dept. of Electrical Engineering
Columbia University
New York, USA
matthias.preindl@columbia.edu

***Abstract*—An air-core inductor is designed and experimentally tested for use in a 3-phase 47kW grid-tied soft-switching inverter. The combination of switching frequencies in the hundreds of kiloHertz and peak currents over 100A, necessary for soft-switching over the entire grid cycle, causes significant iron loss in cored inductor designs. The novel use of air-core inductors in this application, with power levels of 8kW per inductor, eliminates these losses, improving overall converter efficiency. A comparison in design and performance with a ferrite-cored inductor is made and the air-core is shown to be $\geq 0.5\%$ more efficient at rated power, with higher savings at partial power. The design reduces weight while increasing volume to maintain inductance. Radiated electromagnetic interference is analyzed in a simulation and is shown to be benign to the circuit's operation in practice.**

***Index Terms*—air-core inductors, magnetics, power electronics, variable frequency**

I. Introduction

Small, efficient power electronics are a key part of the electrification of global energy use. These electronics typically require magnetics, be they inductors, transformers, or both, to provide everything from galvanic isolation, to filtering, to resonance. However, these magnetics can be difficult to design optimally and often require complex simulations to select interacting parameters such as core size, core material, airgap, and winding structure. Losses in particular can be calculated but are not always accurate, especially when the exciting waveforms are non-sinusoidal, high frequency, or high magnitude [1].

Inductors for electric vehicle (EV) related power electronics are increasing in rating from less than one to tens of kilowatts per inductor. At the same time, the push for power density has driven up switching frequencies [2], [3]. However, reducing volume purely by increasing frequencies is limited by losses in magnetic core materials.

This combination of increasing powers and switching frequencies has led to situations of high magnetic fields that are changing rapidly. For example, in a 3 phase grid tied inverter such as those in [4] switching frequencies of over $1MHz$ are achieved variably throughout the grid cycle. The converter, meanwhile, is being pushed to $> 20kW$ per stage. The amount of energy stored in an inductor increases with the square of the current meaning the cores of potential inductors, which suffer losses that increase non-linearly with both increased fields and frequencies [1], are processing, and losing, much more energy.

One simplification that has been used in other fields is the use of coreless or "air-core" inductors and transformers [2], [5], [6]. These inductors are typically used in high frequency applications, such as radio frequency and chip power supplies, where magnetic materials would otherwise saturate. Some attempts have been made in the power electronics literature for air-core magnetics [7]–[11], but not at current and voltage levels sufficient for EVs.

This paper will explore the performance of air-core inductors under these conditions. They have several advantages that will be exploited in an example circuit: a soft-switching grid-tied inverter. First, the lack of magnetic material means that there is no chance of nonlinear inductance behavior through saturation [12]. For the same reason, there are no core losses. Both the hysteresis loss, caused by nonlinear realignment of magnetic domains, and eddy current loss, caused by induced electric fields in the core itself, are no longer possible. These losses, commonly modeled by variations on the Steinmetz equation [1], [13], are the most complicated to model. The inductor design process is significantly simplified by discounting these equations, which are empirical and accurate over a limited range of operating conditions.

There are several potential drawbacks to air-core inductors that must be addressed before design can begin. Without a core, the magnetic flux is no longer guided and contained; this has several ramifications. The reduced flux density means that the inductance available in a given volume is smaller. However, for the application being considered, an inductance range of just 1-10μH is necessary, which, as will be seen, is easily achievable in a relatively compact size. Although air-core inductors may not be feasible for designs with low switching frequencies or high inductances, they should not be discounted for situations with medium to high frequencies and high powers.

A second potential issue is the increase in copper loss. In order to achieve the same inductance as a cored design, an air-core inductor will require more turns and/or more area. This means an increase in the length of copper, increasing both the DC and frequency-dependent resistance, as well as potentially increasing proximity effects [14]. The implication of this is

that the decrease in core losses must be greater than the increase in winding losses so that the net loss is lower overall. For simplicity, this paper will not consider toroidal inductors, only solenoidal, as they tend to require longer lengths of wire for a given inductance.

Lastly, the absence of a core results in increased electromagnetic interference (EMI) caused by the unconfined magnetic field. Most crucially, this EMI must not disrupt the proper actuation of the power electronic circuit from which it is generated. Nominal circuit operation will ensure that there is no feedback loop that may damage the electronics or interfere with control. If it can be shown that electronics that are not additionally hardened against EMI can still operate effectively with an air-core inductor in close proximity, then other EMI concerns can be mitigated with common techniques such as metallic shielding around the converter as a whole.

This paper presents the design and operation of an air-core inductor for use in a softswitching grid tied inverter. Comparisons will be made with a ferrite-cored inductor of similar inductance. The requirements and design are shown in Section II. Next, a simulation is conducted using Ansys Maxwell to examine the magnetic fields in Section III. The experimental results are provided in Section IV. Finally, in Section V, the paper is concluded.

II. Inductor Requirements and Design

A. Inductance

The first parameter to choose for the inductor is the required inductance itself. Three identical inductors will be used in the power factor correction (PFC) stage of an EV charger as described in [4]. This circuit topology, shown in Fig. 1, differs from a traditional inverter by the connection of the DC minus to the capacitor star point. This decouples the switching instances of the phases and allows for single phase analysis to describe the system.

The relationship between inductor current ripple ΔI and switching frequency f_{sw} is given by

$$f_{sw} = \frac{D(1-D)V_{DC}}{\Delta I L} \tag{1}$$

where D is the duty cycle, V_{DC} is the DC bus voltage, and L is the filter inductance to be determined. It is this relationship that will be manipulated to ensure soft-switching.

The inductance value is chosen such that soft-switching will be maintained in all operating conditions under variable switching frequency operation [4]. It will be assumed that the DC bus value is a constant and set such that the duty cycle range, which depends on the ratio of the bus to the grid voltage magnitude, is roughly between $[0.1, 0.9]$. This will prevent the main control parameter, D, from saturating.

The ripple needed to soft-switch is determined by

$$\Delta I = \alpha(I_{grid} + I_{Lim}) \tag{2}$$

where α is a parameter set at 2, I_{grid} is the sinusoidal grid current, and I_{Lim} is a parameter set such that there is enough excess ripple to soft-switch the MOSFETs. The value of

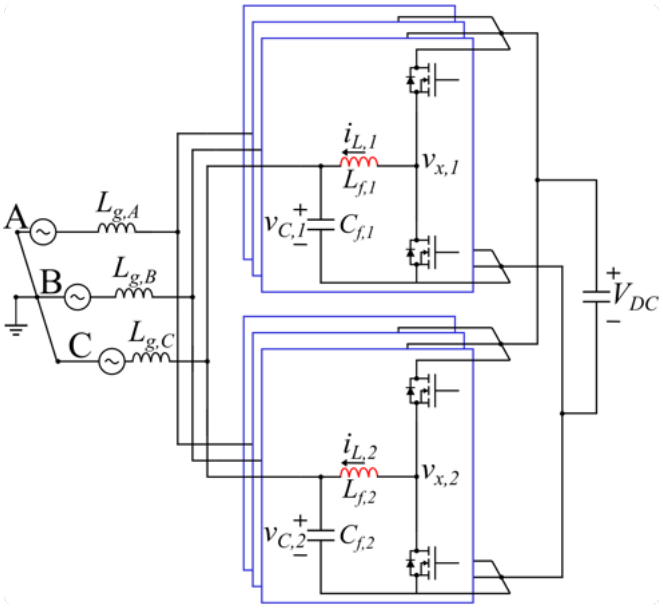

Fig. 1: Circuit topology of the EV charger stage with the designed inductor highlighted in red.

I_{grid} will be determined by the specifications of the converter under consideration. For example, if using a European 400V grid at 50Hz, to achieve 25kW the grid current needs to be approximately 51 A_{pk}.

To determine the necessary inductance (1) can be solved for L and, using the above values, the maximum ripple, which for real power occurs at the peaks of grid voltage, can be compared to the inductance. The lower bound on the minimum switching frequency is set by the top of the audible range. Meanwhile, switching frequencies are limited from above by duty cycle distortions that arise when rise, fall, and dead times become a significant portion of the pulse time, around 600kHz.

A value of 8-10μH operating with a target bus of 800V provides a good margin for operation in the 40-50kHz range at maximum current in a 25kW converter. Inductance values that are smaller than calculated using this procedure will simply provide excess current ripple. Although this is not necessarily optimal for overall efficiency, it will ensure soft-switching operation throughout the grid cycle. Having a target range instead of a specific value will allow for inductance variation that inevitably arises when manufacturing magnetics.

B. Air-Core Design

The inductance of an air-core inductor is described by the empirical Wheeler formula [15]. It is traditionally given by

$$L = \frac{a^2 n^2}{9a + 10b} \tag{3}$$

where L is the inductance in μH, a is the radius, and b is the length of the inductor, both given in inches. The formula assumes a single winding layer, does not consider spacing between windings ($p = d$), and is accurate for $b > 0.8a$. To simplify analysis, these assumptions will be adopted for the

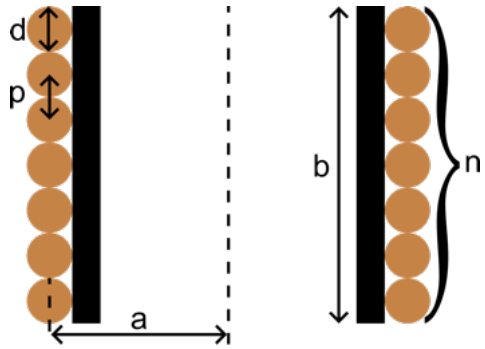

Fig. 2: Key design parameters of an air-core inductor shown in cross section.

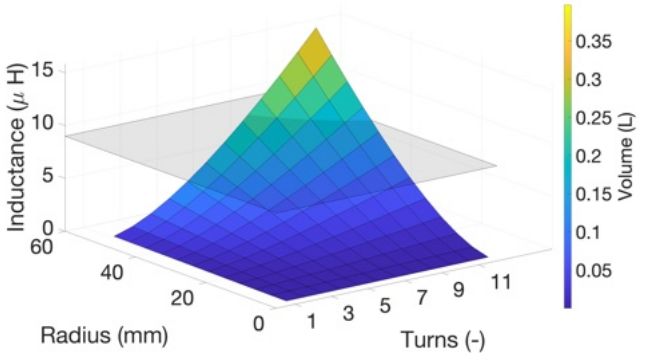

Fig. 3: The optimized Wheeler equation showing L vs. a and n, along with the desired $9\mu H$ of plane of inductance.

remainder of the air-core design. A sketch of the design with relevant parameters is shown in Fig. 2.

The air-core is designed with the primary goal of maximizing efficiency. Without a core, the only source of loss is the windings themselves. Resistive losses can be modeled by

$$P_L = I^2 R(\omega) \tag{4}$$

where I is the current in the conductor and $R(\omega)$ is the frequency dependent resistance. Three major phenomena are known to affect $R(\omega)$ and therefore the resistive losses. The simplest is the DC component that is purely based on the geometry and type of conductor.

There are two frequency-dependent effects that increase the resistance of a wire when carrying alternating currents. First, in the skin effect, alternating magnetic fields generate eddy currents that force the conducting current into an annular "skin" of depth $\delta = \sqrt{\frac{2\rho}{\omega\mu}}$ where μ is the permeability of the material and ρ is its resistivity. Second, the proximity effect describes the tendency of currents in adjacent wires to bundle, again because of eddy currents. Both effects are summarized in the Dowell equation [16], which describes the change in resistance as frequencies increase.

These effects are commonly mitigated through the use of many small, individually isolated wires that are bundled to form Litz wire. To reduce the proximity effect, the strands are twisted within the wire, exposing each wire to different electromagnetic fields. The use of this wire, while more expensive, greatly reduces the frequency dependent effects in the range of interest, thus improving efficiency.

The equations describing these mechanisms can be formally incorporated into an optimization problem to solve for the minimally resistive inductor at a given inductance as is done in [17]. However, a much simpler approach will be taken here that will result in only a minor deviation from the previously calculated optimum.

The idea is to maximize the inductance of an air-core inductor for a given wire length assuming a given wire diameter. All of the loss mechanisms described above are directly dependent on the length of the conductor. By minimizing this length for a given inductance, all forms of loss are mitigated.

To do this, the substitutions $a = \frac{w}{2\pi n}$ and $b = nd$ are made into (3), resulting in

$$L = \frac{w^2 n}{9(2\pi w) + 10d(2\pi n)^2}, \tag{5}$$

where w is the total length of wire.

Setting the derivative of L with respect to the number of turns equal to zero results in a point of maximum inductance and the value of n that achieves it. Using this value and some algebraic manipulations, an optimal "shape ratio", the ratio of inductor length to diameter, of $b/2a = 0.45$ is derived. This is close to the ratio of $b/2a = 0.408$ in [17] and the air-core rule of thumb of "radius equal to length". It is also notable that the optimal point found is in a broad, shallow minimum, meaning that small deviations from the reported optimal shape ratio will not result in large resistance changes.

The behavior of (3) with a fixed shape ratio of 0.45, is shown in Fig. 3. The target inductance of 9μH is given by the gray plane. Only a full turn of wire encloses area and provides inductance quantifiable by the Wheeler equation. Therefore, the resulting inductance changes in steps as the integer number of turns increases. To further narrow the inductance selection, the coloring in Fig. 3 is based on the total volume of the air-core cylinder. Solenoids with more turns but smaller radii have a lower volume and thus are more desirable.

The final air-core inductor used was chosen with a value of $9.2\mu H$ and has a radius of 42mm, a height of 40mm, and 10 turns. A small change (2mm) in the effective radius due to the thickness of the wire is taken into account. The Litz wire is equivalent to 10AWG and supports frequencies up to 800kHz, well within the operating range of this converter.

C. Cored Inductor Comparison

The cored inductor against which the air-core will be compared was designed following the efficiency-volume optimization process described in [4]. The result is a compact design with two paralleled E42/21/20 3F36 Ferroxcube cores, a 6.2mm airgap, and 8 paralleled turns of Litz wire. It has an inductance of $8.3\mu H$. A MnZn ferrite core was chosen because of its availability and its combination of high permeability

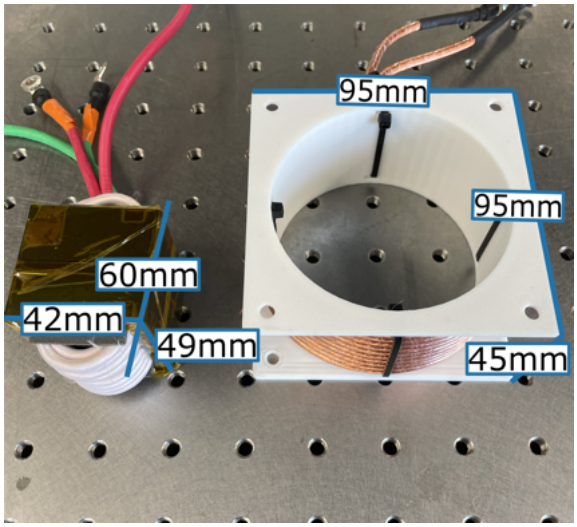

Fig. 4: Physical prototypes of the cored and air-core inductors.

and low loss. Other materials, such as carbonyl iron and NiZn ferrite, have lower permeability and are intended for higher frequency operation than will be used here. The air- and ferrite-core inductors being compared are shown in Fig. 4.

In addition to the copper loss mechanisms described above, the cored inductor experiences iron losses. These come in two forms, induced eddy current and hysteresis losses. The structure of the ferrite means that the hysteresis losses dominate. Both of these magnetic losses are modeled by the Steinmetz equation, a curve fitting equation that relates the power loss density to the frequency and magnetic flux density as in

$$P_v = k f^a B^b. \tag{6}$$

The equation, while widely used, is not accurate for non-sinusoidal excitations. This can be partially compensated for using the improved generalized Steinmetz equation [13], but even this does not account for DC bias currents. As will be shown, the currents seen by the inductors are sawtooth waveforms that vary in magnitude, frequency, and bias, making them particularly difficult to model using any form of the Steinmetz equation.

Overall, the volume of the cored inductor is 0.123L while the air-core is 0.255L, or roughly double. The weight, meanwhile, is reduced from 359g to 248g or approximately 30% thanks to the removal of the core and despite the increase in wire.

III. Simulation

To compare the magnetic properties of the two inductors, both were simulated in Ansys Maxwell. The inductors were excited with a $50kHz$, $150A_{Pk}$ current that represents the highest peak ripple currents experienced by the inductors during operation.

Fig. 5a shows the distribution of the magnetic flux density in the EE core inductor as a result of the applied excitation. As can be seen, despite the airgap, which is necessary to forestall

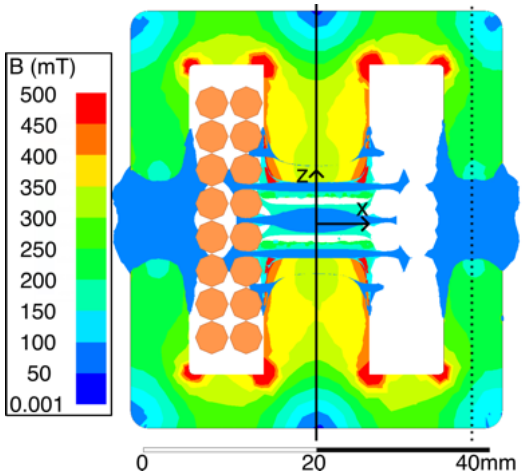

(a) Cored inductor simulation of magnetic flux density

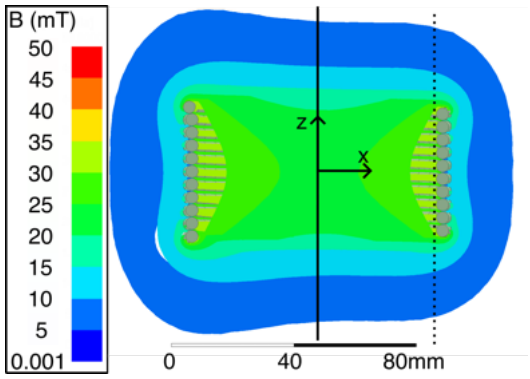

(b) Air-Core inductor simulation of magnetic flux density

Fig. 5: The solid and dashed lines represent the central and offset axes plotted in Fig. 6. Note the differences in B-field and length scales.

saturation of the core, the magnetic field density within the core is high, with parts exceeding $500mT$. The increased flux at the corners, caused by fringing fields, represents locations of high loss, which limit the operation of the core. This is at the worst-case grid operating point in terms of magnetic flux and will change with the phase of the grid.

Further increasing the airgap beyond the 6.2mm (already large) used here would reduce the flux density in the core, reducing inductance and loss. In this regime, the practicality of the core as a guide for flux becomes less evident. As the airgap increases, the effect of the core on the inductor decreases and a cored inductor approaches an air-core.

In order to maintain practical use with a core, it is typical to increase the core volume rather than the airgap. However, increasing the volume to sufficiently reduce the magnetic flux density to prevent high loss density would bring it to a volume comparable to that of the air-core inductor. At which point, the air-core core inductor should be considered equally with the cored inductor in terms of inductance and power density.

The lack of core results in a lower overall magnetic flux density, as seen in the 10x lower scale of Fig. 5 as compared

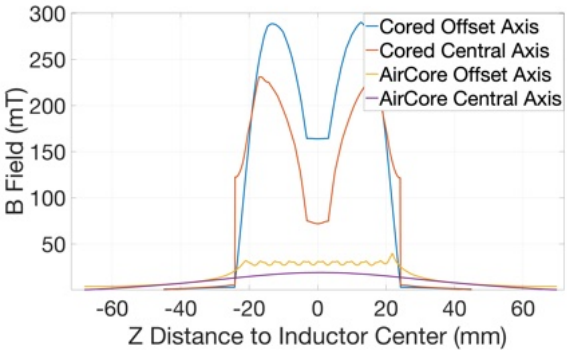

Fig. 6: Magnetic flux density comparison between cored and coreless inductors along two slices in the z direction.

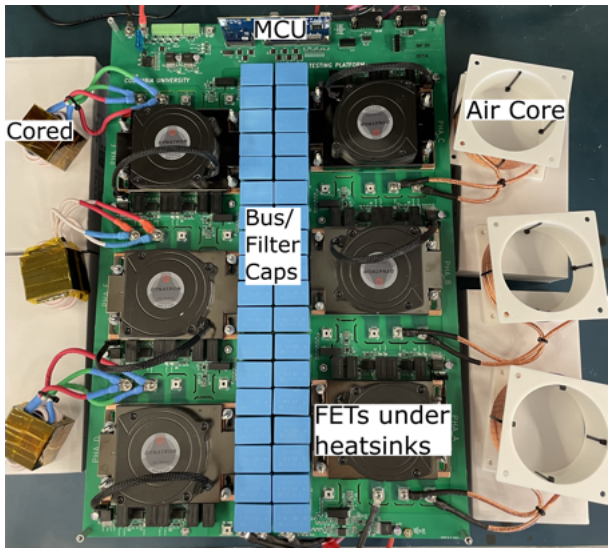

Fig. 7: Software-defined power electronics testing platform, showing the PCB and attached inductors.

to Fig. 5a. However, the magnetic field also drops off more slowly. A comparison of slices of the magnetic fields of the two inductors on the same scale is shown in Fig. 6. Two slices are taken, one along the central axis of each inductor for easy comparison and the other along an offset axis. The cored inductor's offset axis was chosen in the middle of one of the side prongs, while the air-core's is directly adjacent to the wires, where the magnetic fields are expected to be strongest. As expected, the peak of the cored inductor is much higher but is better contained. However, while the B-field of the air-core persists for twice as long it does so at relatively low levels.

IV. Experimental Setup and Results

In order to compare the performance of the two inductors, both are placed into the same circuit and operated under the same voltage and current conditions. The circuit consists of two parallel, interleaved three phase PFC stages, as in Fig. 1, made to interface with the European grid of $400V_{LL}$.

The software-defined power electronics testing platform used for experimental verification is shown in Fig. 7. The PCB

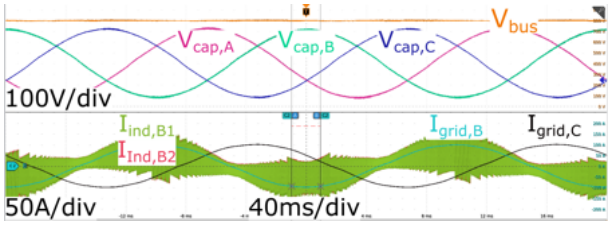

(a) Results using the air-core inductor showing the current ripple and resulting grid current while operating at $47kW$.

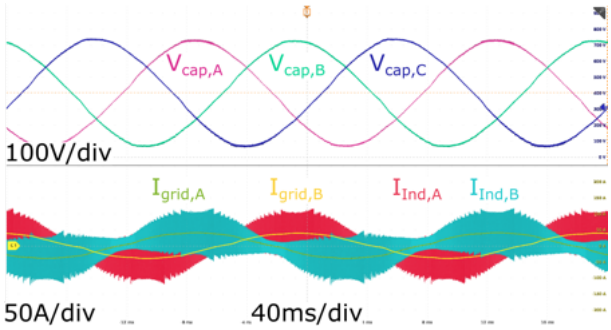

(b) Results using the cored inductor at 20kW, non-interleaved.

Fig. 8: Capacitor and bus voltages and grid and inductor currents during operation.

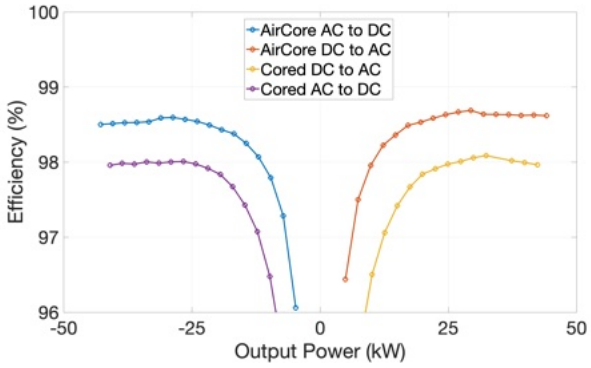

Fig. 9: Efficiency comparison between air-core and cored inductor setups as measured with a power analyzer.

has six half-bridge subcircuits with a common DC bus that can be configured as desired by attaching different magnetics and adjusting the control. For compactness and comparison purposes the figure shows three cored and three coreless inductors attached. However, when testing the interleaved circuitry, all six half bridges would have either air-core or cored inductors.

As can be seen, the inductors are placed adjacent to the PCB and, despite the proximity, the EMI generated in both cases is not enough to interfere with the proper operation of the circuit. This includes the digital gate-drive signals, analog sensor signals, and the micro-controller. A theoretical prototype could be packaged with a shielded case, which would block EMI from propagating and affecting any other components.

Oscilloscope waveforms using the air-core inductors are

shown in Fig. 8a while those for the cored inductor are in Fig. 8. Both show capacitor voltages, grid currents, and inductor currents. The air-core results of Fig. 8a in particular show interleaved results with the inductor currents overlaid but 180 degrees out of phase to partially cancel the ripple. The cored waveforms are shown to demonstrate the similarity in operation of the two inductors and the flexible nature of the setup, in which just one half of the converter can be used.

Fig. 9 shows the difference in efficiency as power flow increases both to and from the battery. As can be seen, the air-core significantly outperforms the cored inductor across the entire range. The percent increase in savings is largest at lower powers but is still significant at high powers. This could be because of increased savings at higher frequencies, typical at lower powers. As an example of absolute savings, the air-core reduces loss by 235W at an output power of 40kW.

V. Conclusion

This work shows the feasibility of air-core inductors in power electronics designs for variable-frequency converters at power levels required by EV chargers. Their use under high currents and frequencies simultaneously has not been explored previously in the literature. A simple design principle, the ratio of height to radius, is presented to create efficient air-core inductors at a desired inductance.

The air-core inductors are tested in hardware under variable switching frequencies and compared with a cored inductor. They have been shown to increase converter efficiency by 0.5% at rated power and even more at lower powers where higher frequencies are needed. Compared with the cored design, the volume and extent of the magnetic field are doubled while the weight of the air-core is decreased by 30%. Future work may include comparisons with lower permeability cores and methods to decrease volume. In addition, boundary conditions for the use of air-core as a substitute for cored inductors based on frequency and current magnitudes will be investigated.

References

[1] T. Guillod, J. S. Lee, H. Li, S. Wang, M. Chen, and C. R. Sullivan, "Calculation of ferrite core losses with arbitrary waveforms using the composite waveform hypothesis," in *IEEE Applied Power Electronics Conference and Exposition (APEC)*, Mar. 2023.

[2] M. Solomentsev and A. J. Hanson, "At what frequencies should air-core magnetics be used?" *IEEE Trans. on Power Electronics*, vol. 38, no. 3, pp. 3546–3558, Mar. 2023.

[3] D. J. Perreault, J. Hu, J. M. Rivas, *et al.*, "Opportunities and challenges in very high frequency power conversion," in *IEEE Applied Power Electronics Conference and Exposition*, Washington, DC: IEEE, Feb. 2009.

[4] M. Jahnes, L. Zhou, Y. Fahmy, and M. Preindl, "A peak 1.2-MHz, >99.5% efficient, and >10-kW/l power dense soft-switched inverter for EV fast charging applications," *IEEE Trans. on Transportation Electrification*, vol. 10, no. 3, pp. 5520–5532, Sep. 2024.

[5] A. Mediano and F. J. Ortega-Gonzalez, "Class-e amplifiers and applications at MF, HF, and VHF: Examples and applications," *IEEE Microwave Magazine*, vol. 19, no. 5, pp. 42–53, 2018.

[6] C. R. Sullivan, D. V. Harburg, J. Qiu, C. G. Levey, and D. Yao, "Integrating magnetics for on-chip power: A perspective," *IEEE Trans. on Power Electronics*, vol. 28, no. 9, pp. 4342–4353, Sep. 2013.

[7] R. T. Naayagi and A. J. Forsyth, "Design of high frequency air-core inductor for DAB converter," in *IEEE International Conference on Power Electronics, Drives and Energy Systems (PEDES)*, Dec. 2012.

[8] U. Pratik and Z. Pantic, "Design of variable air-core coupled co-axial solenoidal inductors," in *IEEE Energy Conversion Congress and Exposition (ECCE)*, Oct. 2022.

[9] W. Liang, L. Raymond, and J. Rivas, "3-d-printed air-core inductors for high-frequency power converters," *IEEE Trans. on Power Electronics*, vol. 31, no. 1, pp. 52–64, Jan. 2016.

[10] E. Asahina, M. Fukuoka, I. Masuda, A. Nagai, K. Maeda, and M. Ishitobi, "Structure of air-core power inductor with high energy density and low copper loss," *IEEE Trans. on Magnetics*, vol. 59, no. 11, Nov. 2023.

[11] C. D. Meyer, S. S. Bedair, B. C. Morgan, and D. P. Arnold, "High-inductance-density, air-core, power inductors, and transformers designed for operation at 100–500 MHz," *IEEE Trans. on Magnetics*, vol. 46, no. 6, pp. 2236–2239, Jun. 2010.

[12] R. A. Salas and J. Pleite, "Simulation of the saturation and air-gap effects in a POT ferrite core with a 2-d finite element model," *IEEE Transactions on Magnetics*, vol. 47, no. 10, pp. 4135–4138, Oct. 2011.

[13] K. Venkatachalam, C. Sullivan, T. Abdallah, and H. Tacca, "Accurate prediction of ferrite core loss with nonsinusoidal waveforms using only steinmetz parameters," in *IEEE Workshop on Computers in Power Electronics*, Jun. 2002, pp. 36–41.

[14] P. Murgatroyd, "The optimal form for coreless inductors," *IEEE Trans. on Magnetics*, vol. 25, no. 3, pp. 2670–2677, May 1989.

[15] H. Wheeler, "Simple inductance formulas for radio coils," *Proc. of the Institute of Radio Engineers*, vol. 16, no. 10, pp. 1398–1400, Oct. 1928.

[16] P. Dowell, "Effects of eddy currents in transformer windings," *Proc. Inst. Electr. Eng. UK*, vol. 113, no. 8, p. 1387, 1966.

[17] T. Ibuchi and T. Funaki, "A study on copper loss minimization of air-core reactor for high frequency switching power converter," in *IEEE International Symposium on Power Electronics for Distributed Generation Systems (PEDG)*, Jul. 2013.